Electrical, Thermal, and Mechanical Characterization of Hot Coined Carbon Fiber Reinforced Pure Aluminium Composites

Mostafa Eid[1] · Saleh Kaytbay[1] · Ahmed El-Assal[1] · Omayma Elkady[2]

Abstract

Poor interfacial structure and severe agglomerations of carbon fiber (CF) are significant problems that face carbon fiber reinforced aluminium (CF/Al) composites. Thus, CF was surface modified with nano copper particles (Cu) to overcome these problems. Two groups of CF/Al composites (uncoated and coated) at different weight percentages of reinforcement (0, 5, 10, 15, and 20) were fabricated using the planetary ball milling method and then uniaxially hot coined at 550 $^{\circ}$C under 700 MPa. The results showed that CF refined the crystallite size of the Al matrix, and no Al_4C_3 or Al_2Cu were detected in XRD patterns. The density and thermal expansion of composites reduced with increasing CF percentage in all samples. The electrical and thermal conductivities are improved up to 10 wt% of uncoated reinforcement and 15 wt% of coated one. The mechanical test results revealed that by increasing CF, the compressive strength of composites decreased while the wear properties improved for both groups. Cu deposition on CF improved the bonding between reinforcement and matrix, producing composites with better interfacial bonding, fewer agglomerations and porosity, and higher values of the properties of the composites.

1 Introduction

Recently, efficient thermal management has become tremendously important for electronic devices to avoid overheating generated in electronic package applications, inducing efficiency degradation and systems failure. Therefore, developing materials characterized by high thermal conductivity and a low coefficient of thermal expansion (CTE) is essential to satisfy the electronic device thermal dissipation requirements [1–4].On the other side, the world interest in high strength, lightweight and anti-corrosion materials which are used for aerospace, vehicles and defence applications has tremendously increased because of their potential to enhance energy efficiency and reduce fuel consumption and CO_2 emissions.

Aluminium matrix composites (AMCs) are considered promising materials used in many industrial applications. Although Al element has unique features such as low density, low melting point, abundant, good formability, and a high potential for recycling, its relatively high CTE, low mechanical properties and low wear resistance at high temperatures hinder its use in thermal and mechanical applications. So the integration of ceramic reinforcements into the Al matrix is an efficient way to overcome these limitations [5–7]. CF is an excellent material to reinforce Al and its alloys due to its superb properties. CF possesses ultra-high thermal conductivity (800 Wm^{-1}/K^{-1}), remarkable CTE (10–15 ppm/K), high workability, low density (1.75–2.25 g/Cm^{-3}), high tensile strength (2–7 GPa), high young modulus (200–900 GPa) and low-cost material [8]. In addition, CF has not only high mechanical properties but also improves tribological properties of AMC_S[9, 10]. Thus, CF/Al composites are preferred for thermal management materials and transport sectors [8, 11–13]. For example, CF /Al composites have been used to fabricate Hubble Space Telescope

✉ Omayma Elkady
 o.alkady68@gmail.com

1   Department of Mechanical Engineering, Benha Faculty of Engineering, Benha University, Banha, Egypt

2   Powder Technology Division, Manufacturing Technology Department, Central Metallurgical Research and Development Institute CMRDI, Cairo Governorate, Egypt

[14]. Moreover, they are also used to reduce the thermal stress on electronic packages [15, 16]. Despite the excellent properties of CF/Al composites, some challenges hinder the progress of the manufacturing of these composites.

Low wettability and excessive harmful reactions are the main drawbacks that encountered the fabrication of high-performance CF/Al composites and deteriorated their thermal and mechanical properties [11, 17]. The contact angle between Al and CF is $140°$[18].This makes it easy to form pores and agglomerations at the interface due to their significant difference in density and melting points [7, 19]. The metallic coating is usually applied on the CF surface to improve not only the interfacial bonding and wettability but also the properties of composites [20–22]. The electroless coating is the most common technique used in the coating process owing to its simple, few tools used, and uniform coating layers can be obtained [23, 24]. Electroless Cu or nickel (Ni) metals are commonly adapted for CF materials [25–28]. For example, Jiang et al.[29] proved that graphite coating with Cu and Ni could enhance the interfacial structure between two constituents in graphite flakes/Al composites.

On the other side, CF reacts with Al at temperatures above 500 °C to produce Al_4C_3 which is an undesirable intermediate phase, and this reaction increases with an increase in temperatures [30, 31]. This interfacial product negatively affects the thermal and mechanical properties of CF/Al composites [32, 33]. For controlling the harmful reactions, suitable processing methods and processing parameters (time–temperature-pressure) should be chosen. CF/Al composites are manufactured by either liquid state or solid-state techniques [34]. Although liquid-based processes are cost-effective and simple, they require elevated temperature and high-pressure conditions. The segregation of reinforcements and intermetallic phase in these techniques impeded their widespread use [35, 36]. The hot coining technique is usually recommended for CF/Al fabrication because it restricts excessive interfacial reactions owing to their relatively low sintering temperature and uniform fiber distribution in the matrix [33, 35, 37, 38]. Moreover, near net shape can be produced, depending on the appropriate die design. Also, it is a rapid consolidating technique that eliminates the possibility of matrix grain growth, resulting in smaller grain size in composites and subsequently better composite characteristics according to the Hall Petch mechanism. Therefore, it is a motivating point to address fabricating CF/Al composites using a hot coining technique with remarkable thermal and mechanical properties.

To our knowledge, many studies have paid attention to the effect of Ni surface modification on CF/Al composites fabricated by solid-state techniques [22, 39, 40]. Others studied the effect of Cu surface modification on the properties of composites. For example, Urena et al.[41] investigated the interfacial mechanical properties using the nanoindentation technique of Cu coated 2 wt% CF/AA6061 composites fabricated via cold compaction process. The results from their work revealed that nanoindentation is an effective method for measuring the hardness and elastic modulus of composites. They also reported that the hardness and stiffness are increased by electroless copper plating.The effect of Cu coating on CF in wear properties of 2 wt% CF/ AA6061 composites prepared by melting tests of cold compressed powder pellets was also investigated in the previous work [42]. It was observed from this work that the wetting of the deposited coatings favored the distribution of reinforcement in the matrix and lowered the risk of reinforcement being dislodged from the composites.

From the previous literature, Cu surface modification was performed at a low weight percentage of CF in Al alloys and these composites were manufactured by traditional cold compaction technique. However, investigations associated with Cu surface modification at different high weight percentages of CF in pure Al and using the novel hot coining process to fabricate CF/Al composites have not been studied yet. Thus, this research aimed to fabricate uncoated and nano Cu-coated CF/Al composites with high contents of reinforcement by the hot-coining method to study the influence of surface modification and reinforcement weight percentages on the microstructure, density, electrical and thermal conductivities (TC), coefficient of thermal expansion (CTE), hardness, compressive strength, and wear properties of CF/ Al composites. This study is significant because it presents a novel way to produce CF/Al composites with low interfacial reactions and remarkable properties.

2 Experimental Work

2.1 Materials

Commercially available Al powder with an average diameter of 60 μm was used as a matrix, while CF (7 μm in diameter and 100 μm in length) was supplied from Easy Composites Ltd and used as a reinforcement material. The characteristics of the CF used are shown in Table 1. Ammonium hydroxide (NH_4OH), Silver nitrate ($Ag NO_3$), Formaldehyde

Table 1 The properties of CF

Parameter	Value
Density	1.8 gm/Cm^3
Hardness	2.9 GPa
Melting point	3500 °C
Purity	100%
Tensile Strength	3150 MPa
Tensile Modulus	200 GPa

(CH$_2$O, 37%), Potassium sodium tartrate, which is called Rochell salt (KNa C$_4$H$_4$O$_6$.4H$_2$O), and copper sulphate pentahydrate (CuSO$_4$.5H$_2$O) were used as a bath for nano Cu deposition and were purchased from ElNasr Chemical Co. LTD, Egypt.

2.2 Electroless Nano Copper Coating of CF

Before electroless Cu coating of reinforcement, CF was pretreated by two subsequent steps: sensitization and activation. Sensitization is an essential process to remove any impurities on CF surfaces and ensure.

a perfect metal deposition. This can be performed by immersing CF in sodium hydroxide solution using an ultrasonic cleaner for 1 h. After that, the sensitized CF was passed into the activation solution (0.017 mol/L Ag NO$_3$, 300ml/LCH$_2$O) and magnetically stirred in the bath for 15 min. The CF activation process aims to create crater-like impressions to rough ceramic reinforcement for a successful coating process. Finally, activated CF was added to a bath which contains (0.14 mol/L CuSO$_4$.5H$_2$O,0.6.mol/L KNa C$_4$H$_4$O$_6$.4H$_2$O,1.25 mol/L NaOH,200 ml/LCH$_2$O). The pH of the solution was adjusted to about 12 using an alkaline solution. As soon as the solution had become transparent and the CF appeared in bright red, the reaction ended. CF was washed with acetone and water several times between each step and finally dried at 90 °C for 1 h in a muffle furnace. Coated CF was vacuum heated under a hydrogen atmosphere in a tube furnace at 450 °C to reduce the oxidized Cu during the deposition process, according to Eq. (1). Figure 1 shows a schematic representation of the reactions that occurred in the electroless Cu coating process.
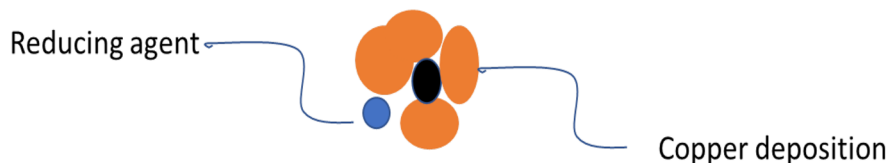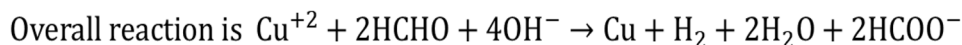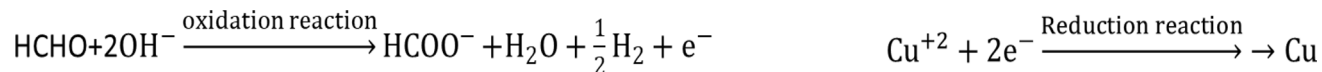
$$CuO + H_2 \rightarrow Cu + H_2O \qquad (1)$$

2.3 Preparation of CF/Al Composites

0,5,10,15, and 20 wt% uncoated and coated CF reinforced Al composites were manufactured by mixing powders in the ball milling machine (PQ-N2 Planetary Ball Mill) according to parameters listed in Table 2. After this step, the two groups of powders were placed into ⌀ 10 mm heat-treated W304 stainless steel. After that, the powders were experienced to relatively low pressure. Then, the die was heated in a muffle furnace at 550 ℃ for 30 min. Then, the die was immediately transferred to a 30-ton uniaxial press and the powders were pressed at 700 MPa for 10 s. Lastly, the samples were allowed to cool naturally in the air to form cylindrical samples. Schematic representation of CF/Al composites fabrication is presented in Fig. 2.

2.4 Composites Characterization

Samples were subjected to metallographic processes through grinding and polishing. After that, composites and powders microstructure were studied using field emission scanning electron microscope (FE-SEM; QUANTAFEG250, Holland), equipped with energy dispersive X-ray (EDAX). X-ray diffraction (XRD, model x, pert PRO PANalytical) using Cu Kα radiation (λ = 0.15406 nm) was also used to

Table 2 Parameters of ball milling

Parameter	Value
Speed	250 rpm
Weight of powders	50 g/vessel
Ball to powder ratio (BPR)	7:1 in uncoated powders
	3:1 in coated powders
Process control agent (PCA)	Hexane
Number of hours	10 h
Ball materials	Zirconia

$$HCHO + 2OH^- \xrightarrow{\text{oxidation reaction}} HCOO^- + H_2O + \frac{1}{2}H_2 + e^-$$

$$Cu^{+2} + 2e^- \xrightarrow{\text{Reduction reaction}} \rightarrow Cu$$

$$\text{Overall reaction is } Cu^{+2} + 2HCHO + 4OH^- \rightarrow Cu + H_2 + 2H_2O + 2HCOO^-$$

Reducing agent

Copper deposition

Fig. 1 Schematic representation of the electroless copper coating reactions

Fig. 2 Schematic illustration demonstrating the steps for preparing CF/Al composites

investigate the phase composition of both powders and consolidated samples during the sintering process. The bulk density of manufactured composites was measured according to Archimedes principles [43]. The theoretical density was calculated using the rule of mixture and the results were compared with experimental values to calculate the relative density. The CTE of composites was measured by a differential dilatometer (NETZSCH DIL 402PC) with a heating rate of 5 °C/min. The averages of CTE were taken between 100 and 350 °C. Material Tester for Metals (PCE-COM 20) is used to evaluate the electrical conductivity of produced samples. The test was performed along with cylindrical samples ($\varnothing$10mm × 4mm) at room temperature. Thermal conductivity was estimated according to the Wiedemann–Franz Law [44]. Microhardness of all composites was observed using Vickers Hardness tester (model HV-1MDT) at an applied load of 300 g for a holding time of 15 s. The compression test was conducted using a universal test machine (WAW-600) according to standard ASTM: E9-09 [45]. The wear test was carried out using a pin-on-disk wear test machine on grounded samples with a 5 N normal load, sliding speed

of 1.45 m/s with a rotational speed of 1400 r.p.m without lubrication. These parameters are chosen according to our previous work [46]. An electronic balance with a resolution of 0.1 mg was used to measure the weight of the samples before and after the test. The specific wear rate was measured through the weight loss of samples divided by the product of the sliding distance and normal load. During the test, the friction force was continuously observed, and friction (COF) was calculated.

3 Results and Discussion

3.1 Powders Characterization

Figure 3a–d show the morphology of Al, CF, activated and coated CF, respectively. Figure 3a reveals that Al powders have an irregular potato shape. In contrast, CF in Fig. 3b has a rod-shaped structure with some epoxy adhered to its surface during its manufacturing process. The activated CF in Fig. 3c indicates that nano-silver particles were successfully
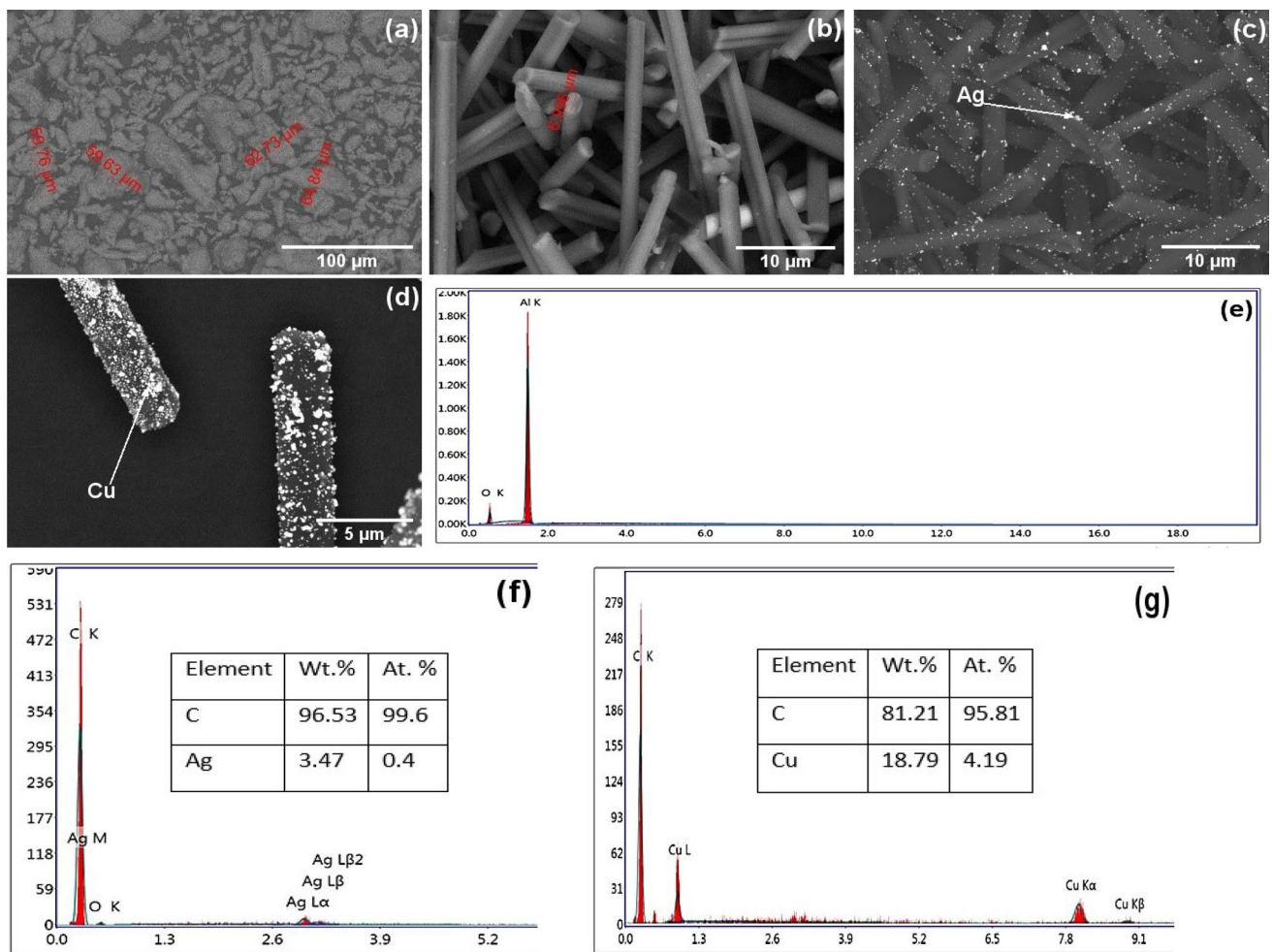
Fig. 3 Morphology of **a** Al powders, **b** CF powders, **c** Activated CF **d** Coated CF, EDAX of **e** Al powders, **f** CF after activation, and **g** CF after Cu coating

deposited and were ready to act as an activation agent for the next process. Figure 3d belongs to the coated CF, which indicates that nano Cu particles have spherical particle shapes that are distributed in a homogenous manner along CF length. The Cu layer is continuous and compacted, showing a good bonding between the nano Cu and CF surfaces. Figure 3e–g are the EDAX analyses of Al and CF powders after the activation and coating processes. Figure 3e shows a small peak of oxygen element in Al analysis, suggesting that the oxygen element was introduced during the milling operation. On the other hand, the analysis of activated and coated CF reveals a complete compositional analysis for both processes, as shown in Fig. 3f and 3g, respectively.

The average length of uncoated and coated CF inside the Al matrix is presented in Fig. 4. The metallic balls during the milling operation have a noticeable influence on the length of reinforcing particles. The particles length after milling was 7.08, 8.33, 9.87 and 12.12 μm for uncoated fiber composites and 6.59, 7.83, 9.07 and 11.54 μm for coated one, which is shorter than that received CF (100 μm). In two groups of composites, more reduction in length of CF particles as CF percentage increases due to a rise in brittle CF number in composites. Also, CF length in coated composites is shorter than in uncoated composites. This can be attributed to the variation in the ball to powder ratio between the two types of groups used in this study. It is reported that the higher ball to powder ratio, the more collision between balls which reduces the efficiency of ball milling, resulting in a badly broken of fibers [47, 48]. It is also seen that the diameter of fiber remains constant. Consequently, the aspect ratio of fiber was 1.01, 1.19, 1.41 and 1.73 for uncoated samples and 0.94, 1.11, 1.29 and 1.6 for coated samples.

3.2 Composites Characterization and XRD

Figure 5 is the SEM image of CF/Al composites detected in the plane perpendicular to the direction of pressing. Figure 5a represents the pure Al, and b,c,d,e belongs to
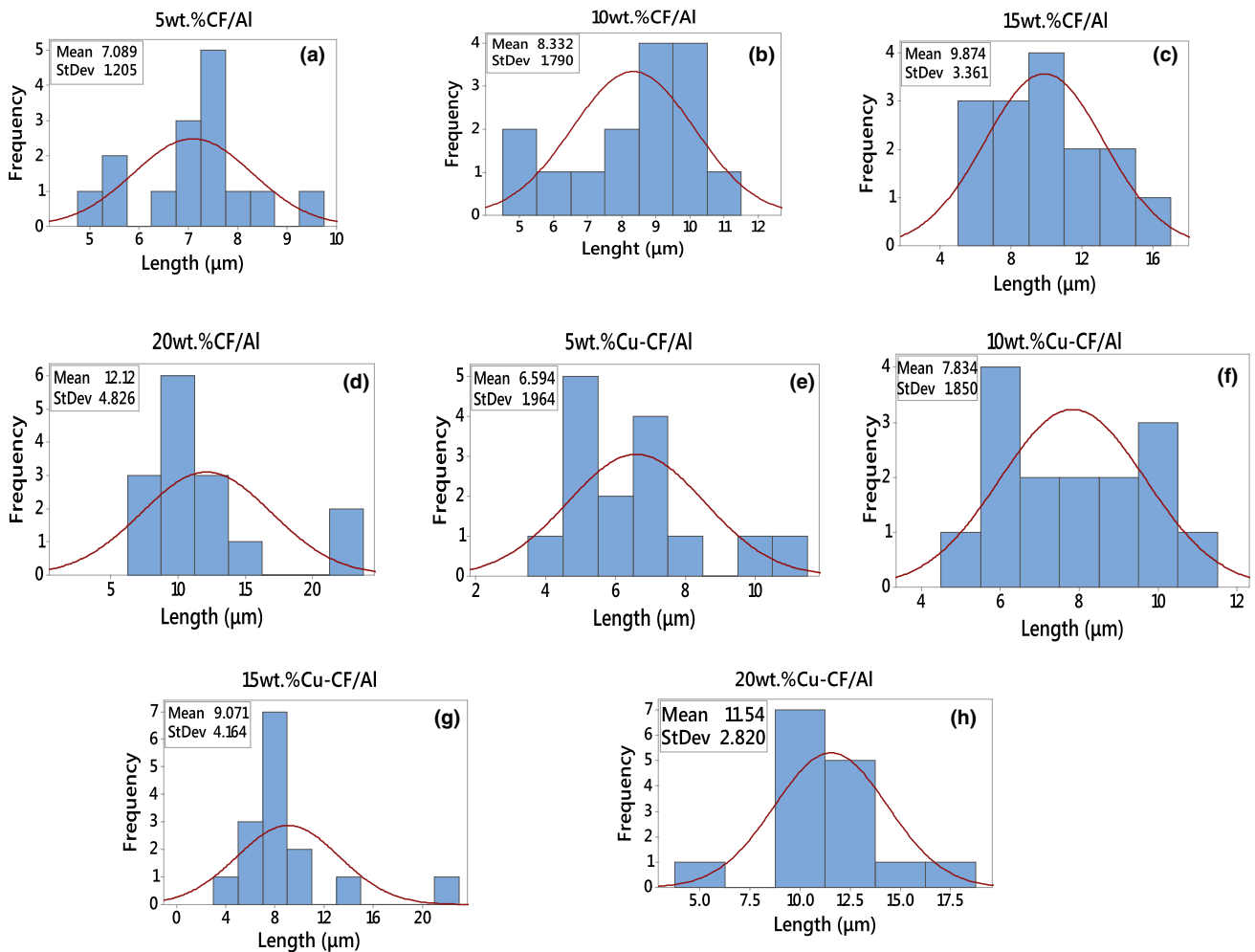
Fig.4 Length distribution of **a** 5 wt%CF/Al, **b** 10 wt%CF/Al, **c** 15 wt%CF/Al, **d** 20 wt%CF/Al, CF/Al, **e** 5 wt% Cu-coated CF/Al, **f** 10 wt% Cu-coated CF/Al, **g** 15 wt% Cu-coated CF/Al, and **h** 20 wt% Cu-coated CF/Al composite

the uncoated CF/Al composites, while f,g,h, i for the Cu coated CF/Al samples. The bright regions are the Al matrix while the dark ones are CF and the white dots correspond to Cu particles. Most CF are broken during the milling process, homogeneously dispersed in the Al matrix, and distributed in the plane perpendicular to the pressing direction due to a uniaxially compressive force during the consolidation process.

It can be seen that Cu nanoparticles migrate towards CF-CF, CF-Al and in the Al matrix. Moreover, coated composites have a better fiber distribution in their structure than uncoated ones. This can be explained by improving the wettability between the CF that has a ceramic nature and the metallic Al matrix by encapsulating the CF with nano metallic Cu, so the surface energy between the two constituents decreases. However, for the uncoated CF/Al composites, the non-wettability problems increase in the collection of CF particles, which appear as agglomerations in the Al matrix.

Higher magnification of the SEM images are demonstrated in Fig. 6 to study the interfacial structure of composites. For uncoated composites, the pores appear at the interface, explaining that interfacial bonding is very weak. On the contrary, in coated composites, good interfacial bonding between the Al matrix and CF where pores are absent at the interface. From the literature, it was concluded that the porosity could cause a drop in the properties of composites. This result indicates that Cu coating is an efficient process to improve bonding between Al and CF. EDAX analysis in Fig. 7 of 10 wt% CF composites is used to check the sample composition at the interface. It can be indicated that Al matrix and CF have been identified at the interface without any contaminations in uncoated CF composites. While in the coated composites, the EDAX results indicate the presence of C, Ag, Cu and Al at the interface, indicating an excellent interfacial adhesion.

The pattern in Fig. 8a revealed that only Al peaks at 2θ $=38.42°, 44.60°, 64.95°, 78.09°$ and $82.30°$ which correspond
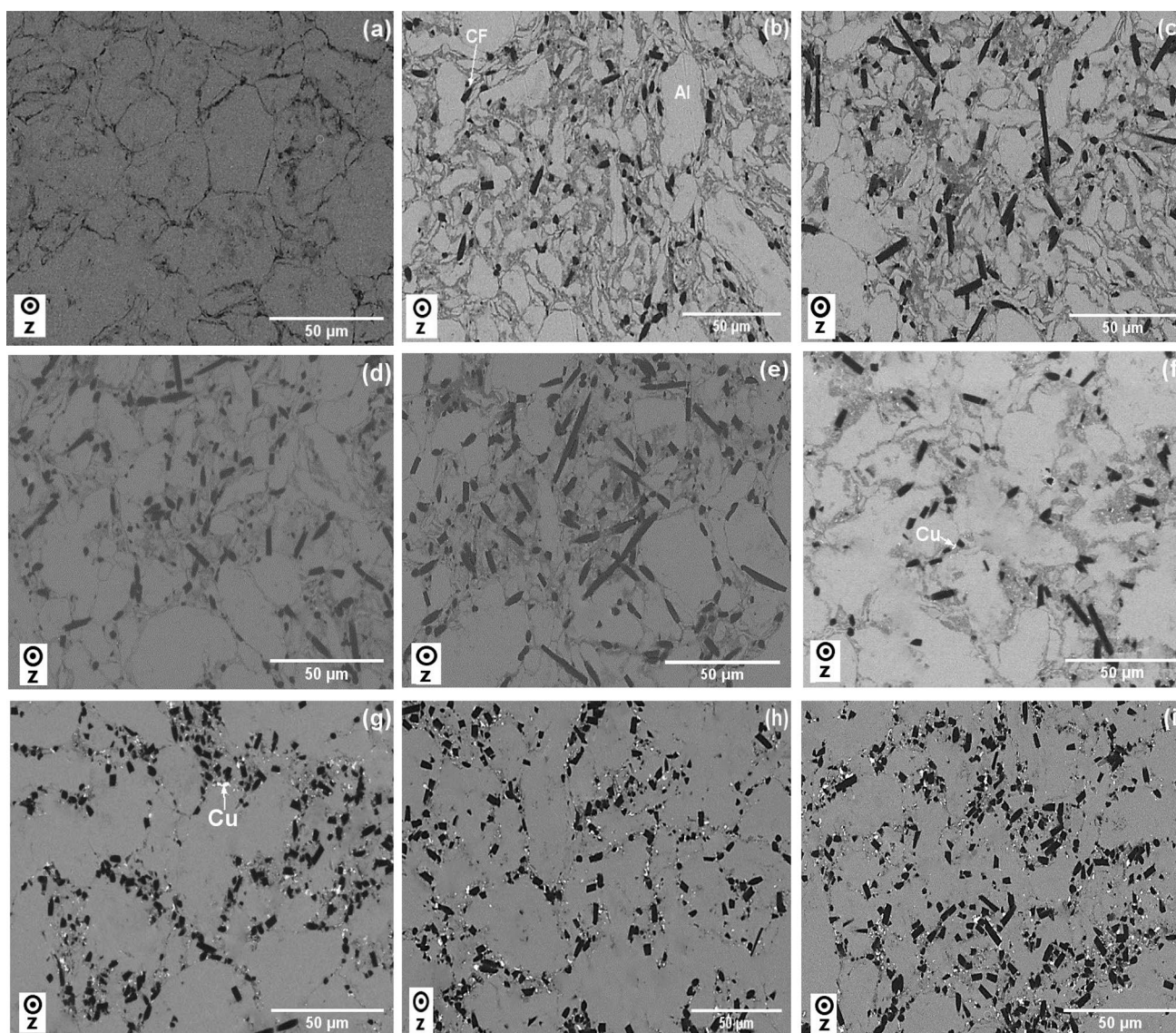
Fig. 5 Microstructure of CF/Al composites observed on the plane perpendicular to pressing direction **a** pure Al, **b** 5 wt% CF/Al, **c** 10 wt% CF/Al, **d** 15 wt% CF/Al, **e** 20 wt% CF/Al, **f** 5 wt% Cu-coated CF/Al, **g** 10 wt% Cu-coated CF/Al, **h** 15 wt% Cu-coated CF/Al, **i** 20 wt% Cu-coated CF/Al composite. (Z axis indicates the pressing direction)

to (111), (200), (220), (311), and (222) crystal planes are observed in Al powders, respectively. While Fig. 8b presents the CF, activated Ag and coated Cu elements in coated CF powder analysis. It is also observed in the study that one small peak for Cu_2O at $2\theta = 36.32°$ correspond to (111) crystal plane. Results of CF/Al composites are presented in Fig. 8c. As expected, the XRD pattern shows the main Al peaks, and the primary CF peak at ($2\theta = 26.2°$) corresponds to (002) crystal plane, which could only be detected in 15 and 20 wt% CF. Moreover, no Al_4C_3 was found in all composites showing that the harmful reactions between Al and CF are absent during the sintering process. For coated composites, the intermediate Al_2Cu phase isn't detected in

the XRD pattern because of the low content of Cu used and our controllable consolidation process. Scherrer's formula in Eq. (2) is used to calculate the crystallite size of the produced composites.

$$d = \frac{0.9\lambda}{B\cos\theta} \tag{2}$$

where d is the crystallite size, λ is the wavelength of the radiation, θ is the Bragg's angle, and B is the full width at half maximum [45]. It is evident from Table 3 that the addition CF and the electroless coating process have a critical role in the crystallite size reduction of composites. This may be attributed to two reasons; the first is the effect of a ceramic
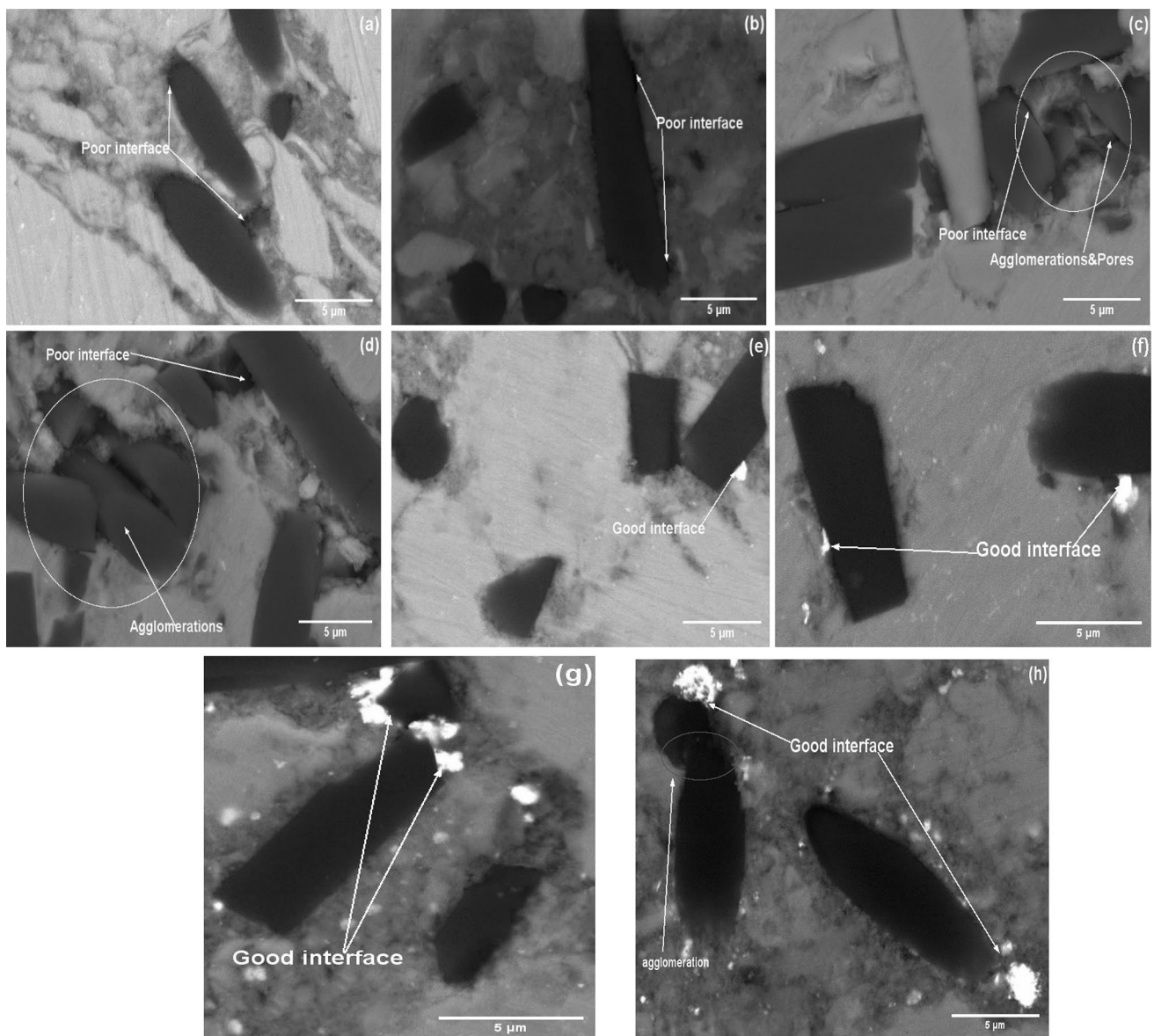
Fig. 6 Microstructure of CF/Al composites with higher magnification **a** 5 wt% CF/Al, **b** 10 wt% CF/Al, **c** 15 wt% CF/Al, **d** 20 wt% CF/Al, **e** 5 wt% Cu-coated CF/Al, **f** 10 wt% Cu-coated CF/Al, **g** 15 wt% Cu-coated CF/Al, and **h** 20 wt% Cu-coated CF/Al composite

nature that acts as internal balls, causing a reduction of particle size. The second is the coating process in which nano Cu particles are mostly distributed on the boundaries of Al grains, as shown in Fig. 5, restricting the growth of Al grains in the consolidation process and resulting in a smooth and fine surface. Therefore, in coated composites, more grains are formed and the grain growth is restrained, thus causing grain refinement. Such a decrease in grain size can positively affect the mechanical properties of composites. Many studies confirmed the enhancement of mechanical properties due to the refining process of grain size [49, 50].

3.3 Density Measurement

The theoretical and experimental densities of the composites along with the corresponding weight fraction of reinforcement are presented in Table 4. It is observed that the measured density of composites decreased with CF contents and was in line with the values obtained by the rule of mixtures. This can be attributed to the low density of reinforcement (1.8 g/cm3) compared to Al (2.7 g/cm3). Additionally, the measured density has lower values than the theoretical one. This difference is attributable to the existence of voids and
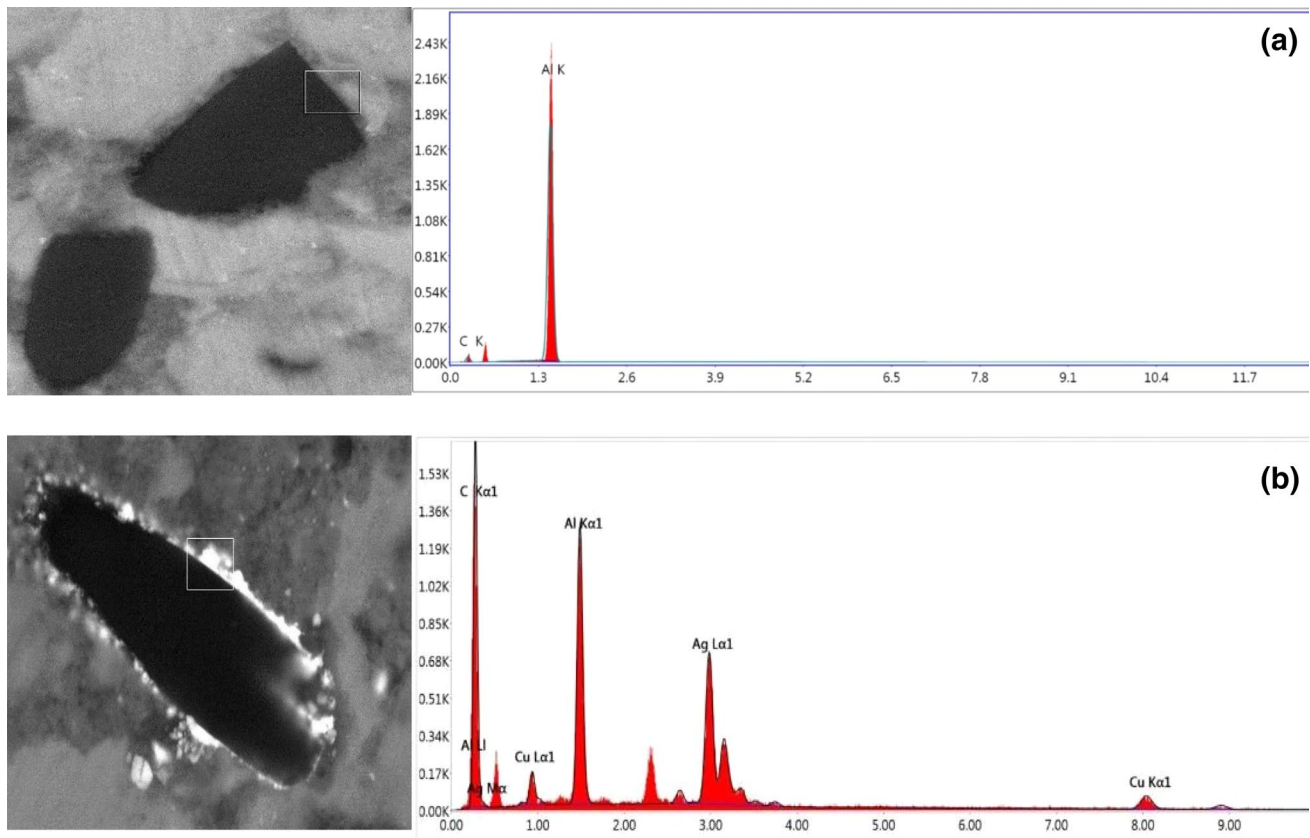
Fig. 7 EDAX analysis of **a** 10 wt% CF/Al composite and **b** 10 wt% Cu-coated CF/Al composite

pores in the composites. The agglomerations and voids are an acute issue in metals matrix composites fabrication. It is hard to disperse CF in Al matrix without forming CF clusters, especially at a higher reinforcement ratio. Examining the degree of voids and agglomerations in this study, in case uncoated composites, the percentage of void in 10 wt% CF composite was 7.48% (see Table 4) and the agglomerations were absent in composite (see Fig. 6. b). These voids then increased significantly to 8.6% and 10.31% in 15 and 20 wt% CF composites, respectively and the agglomerations were prominently shown (see Fig. 6. c and d). However, the pore percentage in 10 wt% Cu-coated samples was 5.1%, which increased to more than 7% in both 15 and 20 wt% CF composites. Moreover, the agglomerations were hardly only detected in 20 wt% CF sample (see Fig. 6.h). These agglomerations could reduce the potential enhancement in the properties of CF composites.

Figure 9 show the effect of both CF content and coating process on the relative density of CF/Al composites. There are two phenomena observed: one is the higher relative density value of the Cu-coated samples than the uncoated ones. This can be explained by the improved wettability between CF and Al due to the nano Cu coating process. The contact angle between Al and Cu is lower than that between Al and CF, so good densification takes place in coated composites. Also, the presence of nano metallic materials such as Cu and Ag facilitates the interconnection between the large micro-Al particles and CF particles, consequently, the densification rate increases. As we said earlier, the pores at the interface are easily filled with nano Cu particles to produce high relative density composites (see Fig. 6).

The second phenomenon is decreasing the relative density by increasing the CF percentage. The higher the content of CF, the more agglomeration areas are formed, which contributes to more gaps in the structure. Fathy et al. [51] reported that incorporating ceramic materials into metallic matrices could form a close network that acts as a barrier of Al diffusion, reducing particles connection and many agglomerations and porosity levels are created during the sintering process. Hard ceramic reinforcements increase the compaction pressure required for composite densification. It is also shown that composites have high relative density values, suggesting that our consolidation technique and high sintering temperature are excellent, resulting in easier diffusion between reinforcement and matrix. Also, the mixed powders are consolidated under both mechanical and thermal loads, so a good interaction between the Al particles and CF occurs, and consequently, low pores are recorded.
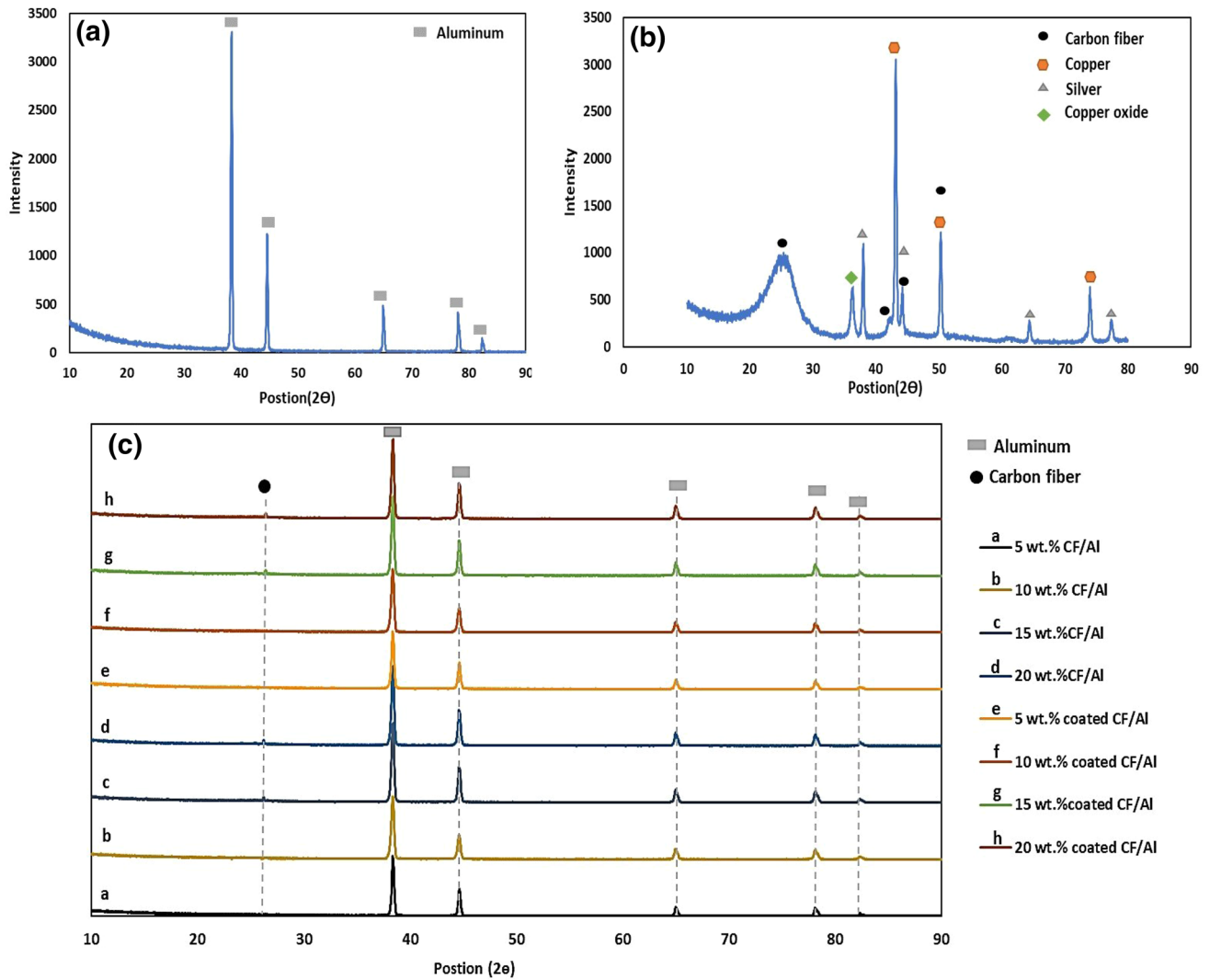
Fig. 8 XRD results of **a** Al powders, **b** CF powders after Cu coating, and **c** CF/Al composites

Table 3 Crystallite size of produced composites

| Wt% CF | Crystallite size (nm) | |
	Uncoated samples	Coated samples
0	39.59	
5	38.25	39.06
10	36.45	24.82
15	35.16	24.26
20	33.89	23.88

3.4 Coefficient of Thermal Expansion (CTE)

Figure 10 shows the CTE of the prepared composites with temperatures varying from 100 to 350 °C. It is noted that the CTE of all composites increases with increasing temperature due to the change in the internal stress of composites.

Table 4 Measured density, theoretical density and void fraction of the sintered samples of CF/Al

Materials	Conditions	Measured density (g/cm3)	Theoretical density (g/cm3)	Void %
Pure Al		2.62	2.7	2.97
5 wt%	Without coating	2.47	2.65	6.8
10 wt%		2.41	2.61	7.48
15 wt%		2.34	2.56	8.6
20 wt%		2.25	2.52	10.31
5 wt%	With coating	2.57	2.697	4.8
10 wt%		2.55	2.694	5.1
15 wt%		2.50	2.691	7.1
20 wt%		2.49	2.69	7.5

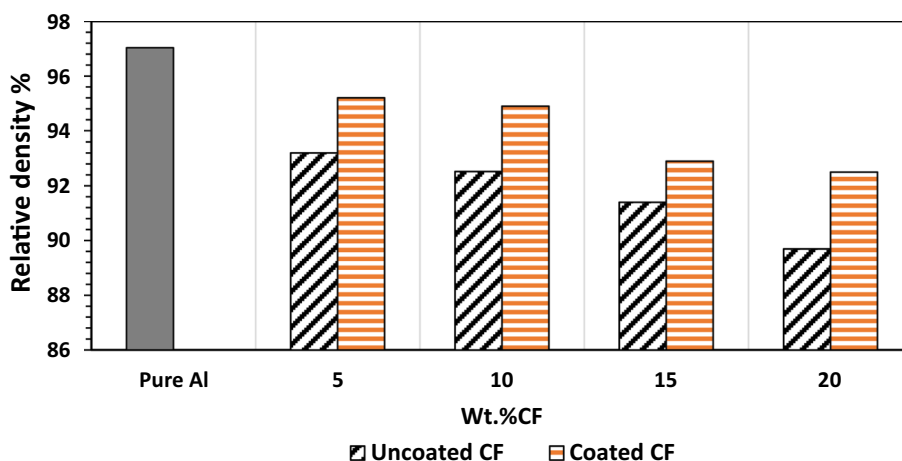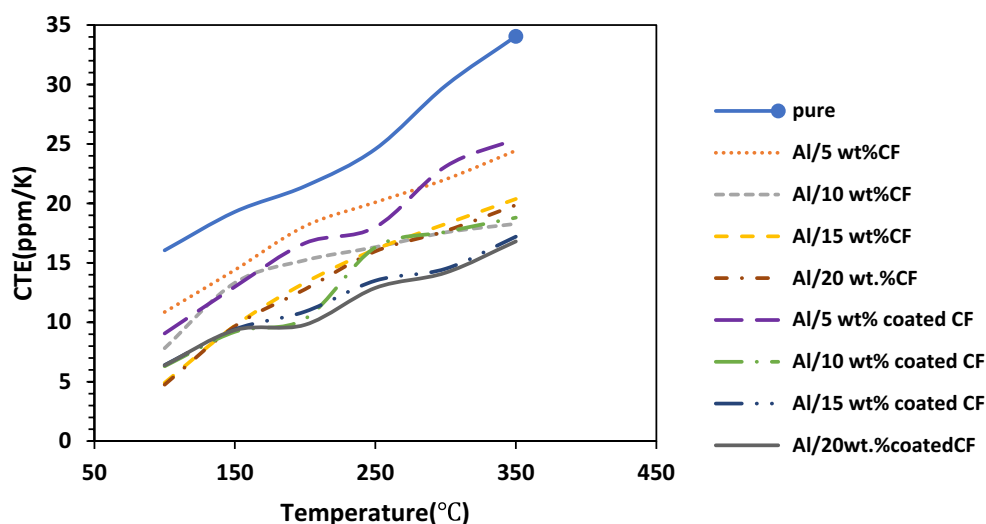**Fig. 9** The relative density of CF/Al composites

Fig. 10 CTE curves of the CF/Al composites against temperatures

Residual stress is generated when composites are cooled from sintering temperature to room temperature during the preparation process due to the large variation in CTE between Al and CF. This residual stress acts as compressive stress on CF and tensile stress on the Al matrix. So, when samples are heated during the test, the tensile stress on the matrix is released, and Al begins to expand [52]. The effect of opposite stresses on CF can be neglected because of the large modulus and strength of CF compared to Al.

On the other hand, Fig. 11 presents the relation between experimental and calculated CTE based on ROM and the turner model [53]. It is noted that the CTE of all CF/Al composites is lower than that of the Al matrix and decreases with an increase in CF. For instance, as compared to Pure Al, the CTE of composites is reduced by 38% and 41.7% at 20 wt% of uncoated and coated CF, respectively. Reduction in CTE values is due to the restriction effect of CF on Al expansion. The electroless coating was an effective way to minimize expansion. Cu-coated CF composites have relatively lower CTE than uncoated composites. This is due to better interfacial bonding that improves Al thermal stability. Low interfacial resistance reduces the CF restriction effect [54]. Additionally, theoretical values are higher than the experimental ones due to the small size of CF particles used in this study which have a large surface area, leading to an increase in direct contact with Al particles at the interface and more thermal expansion reduction. Much reduction in size could be achieved during the milling operation that enhanced the thermal expansion restriction process.

3.5 Electrical Conductivity

The values of electrical conductivity of CF/Al composites are presented in Fig. 12. For uncoated composites, the addition of 10 wt% CF to the Al matrix improves the electrical conductivity of composites from 21.1 MS/m to 25.88 MS/m. Increasing uncoated fiber content to 15 wt% and 20 wt% decreases the conductivity to 17.39 MS/m and 16.89 MS/m,
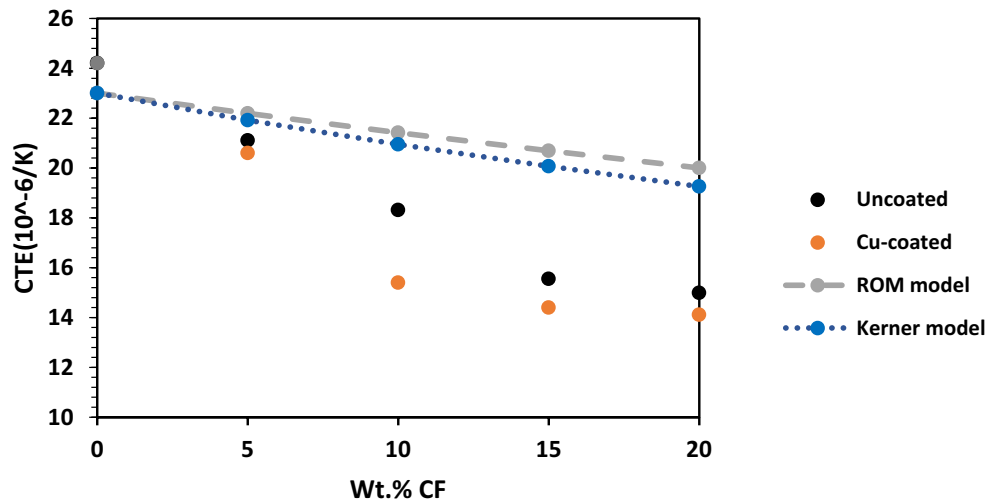
Fig. 11 Comparison between the experimental CTE and the calculated CTE based on the rule of mixture (ROM) and the Turner model as a function of CF percentage in the CF/Al composites
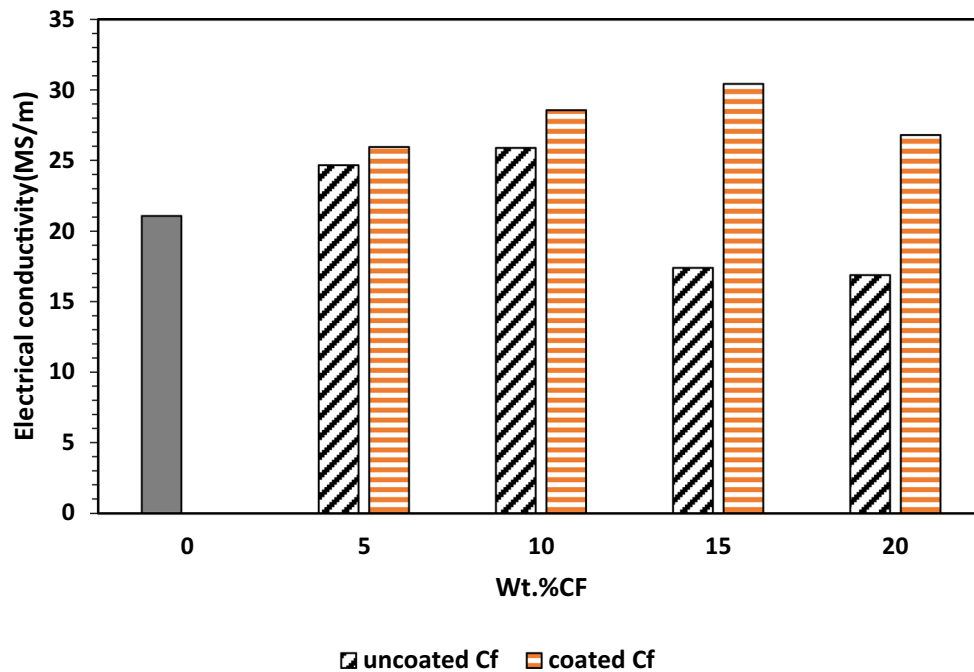

Fig. 12 Electrical conductivity of CF/Al composites

respectively. Meanwhile, the highest electrical conductivity value is 30.43 MS/m for 15 wt% Cu-coated CF/Al composite. Examining the electrical conductivity of CF/Al composites, the existence of conductive reinforcements in the Al matrix increases the number of conductive paths and facilitates the movement of the electrons. Also, the distribution of CF along the Al grain boundary contributes to increasing the conductivity of composites [55]. In fact, the conductivity declines after 10 wt% for uncoated composites owing to the

agglomerations and pores formed at the interface. The conductivity of pores is zero, so their presence in the samples hinders the motion of the electrons and decreases the overall conductivity of the prepared samples [56]. It is stated that defects and low interfacial bonding are the main reasons for restricting electrons motion and increasing electrical resistivity [57, 58]. As mentioned earlier, the number of defects in coated composites was less than that of uncoated ones. So, the electrical conductivity of coated composites continues to

improve after 10 wt% and exhibits better conductivity than uncoated ones. In summary, the addition of CF to the Al matrix has an excellent effect on the electrical performance if only the bonding between matrix and reinforcement is strong and fibers are homogenously distributed in the matrix without any agglomerations.

3.6 Thermal Conductivity (TC)

Figure 13 shows the TC of CF/Al composites containing uncoated and coated CF with different weight fractions. With increasing uncoated fiber from 0 wt% to 10 wt% CF, TC of composite rises from 154.9 $W.m^{-1}.K^{-1}$ to 190.21 $W.m^{-1}.K^{-1}$. The TC values of composite begin to drop with more reinforcement, while Cu-coated CF/Al composites keep improving and increase to 223.6 $W.m^{-1}.K^{-1}$ at 15 wt% CF. CF could enhance the TC of the Al matrix due to the high TC of CF. Reduction in the TC of uncoated composites at 15 and 20 wt% CF and for coated composites at 20 wt% Cu coated CF can be attributed to the creation of voids in the structure, which reduce heat conduction and act as an inhibitor for TC linear growth. The presence of pores decreases TC as the conductivity of the pores is zero, which greatly affects The TC of composites. Pores are considered thermal insulators that have a bad effect on the thermal properties of composites [38, 57]. The electroless Cu coating process could improve the TC of composites due to the high thermal conductivity of the metallic layer itself and its rule to enhance wetting and reduce the interfacial defects, especially at a higher percentage of reinforcement. Cu coating layer could transform the wettability

from between fiber and matrix to two metallic layers, thereby enhancing the TC of composites [59]. Similar observations were reported on TC of CF/Mg composites where the Cu layer significantly enhanced the interfacial bonding and thus improved the TC of composites [60].

3.7 Hardness Estimation

Figure 14 explains the effect of CF and Cu coating on the hardness of CF/Al composites. It shows a continuous increase in the hardness values by increasing the CF content for the nano Cu-coated CF samples. But it improved up to 10 wt% then decreased for the uncoated groups. The microhardness of the Al composites has increased from 0.342 GPa at neat composite to 0.47 GPa at 10 wt% uncoated CF and 0.74 GPa at 20 wt% coated CF /Al composite, with increasing percentages of 37.7% and 114.89%, respectively. The improvement in hardness values may be attributed to an increase in CF particles content, which leads to a decrease in the spacing between particles and an increase in the stress required to induce dislocation movement. This can be proved by the following Equations [61]:

$$\lambda = \frac{4(1-f)r}{3f} \tag{3}$$
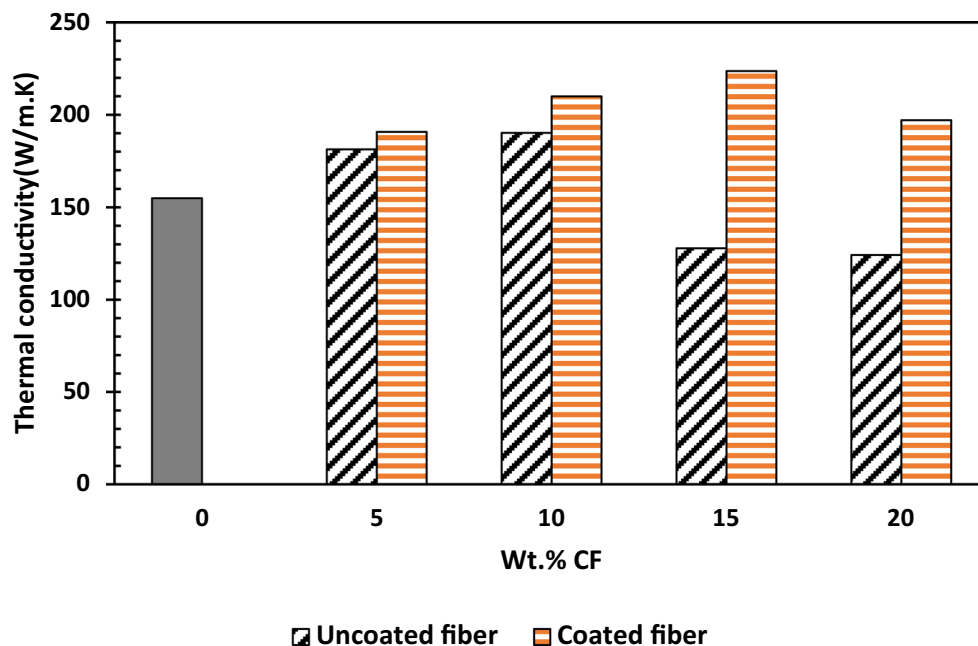
$$\tau_0 = \frac{Gb}{\lambda} \tag{4}$$

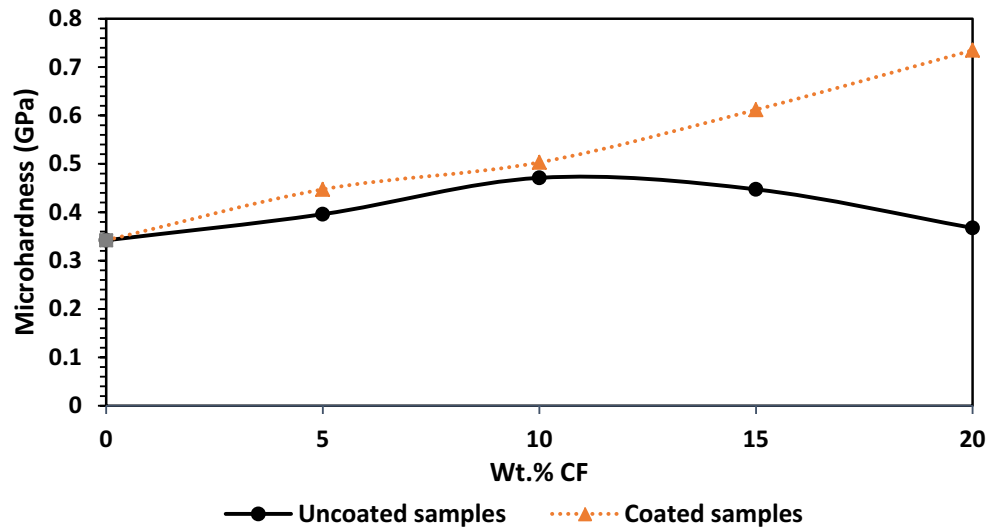**Fig. 13** Thermal conductivity of CF/Al composites

Fig. 14 Microhardness of pure Al and Al composites reinforced with CF with and without Cu coating

where λ is the reinforcement distance,f volume fraction of particles, r is CF radius (assume CF particles is spherical),τ_0 is the shear stress,G is the shear modulus, and b is the burger's vector.

Moreover, incorporating hard ceramic particles into ductile materials with a uniform distribution could reduce grain size, which has a positive effect on the hardness of composites [46]. The reduction in hardness value after 10 wt% uncoated CF may occur because the hardness is affected by other detrimental factors such as aggregation and relative density reduction. Also, coating CF with nano Cu layers causes the reduction of particles and crystallite size, which improves the hardness values according to the Hall Petch equation. The previous result is consistent with studies [11, 62].

The electroless Cu coating role is significant, especially at a higher fraction of reinforcement, where the agglomeration and debonding of uncoated composites are present. By comparing the two groups, the microhardness of coated composites is clearly enhanced by 36.82% and 99.9% at 15 and 20 wt% CF compared to uncoated composites, respectively. The electroless Cu coating could prevent the non-homogeneity, agglomerations of reinforcement in the matrix and refine the grain size of composites. Thus, the ability of the composite to resist indentation increased. Urena et al. [42] stated that Cu coating caused an improvement in hardness for Al composites due to metastable precipitated phases.

3.8 Compression Test

The compression stress–strain diagram of sintered specimens is shown in Fig. 15. The effect of two parameters on compressive strength and ductility of composites is studied in Table 5. It is shown that the strength of the base material is higher than its composites. For instance, when 20 wt% CF was added into the Al matrix, compressive strength was reduced by 34.18% for uncoated composites and 21.56% for coated composites compared to that of pure Al. Fracture mode, presence of porosity, refining grain size and uniform distribution of reinforcement are variables that affect compressive strength value [56, 63, 64]. CF could convert the fracture system from ductile to fracture mode, reduce the relative density of the Al matrix and increase porosity and agglomerations. Pores and agglomerations are considered stress concentration regions where CF is easily broken in these areas under compressive force. These phenomena could vanish the positive effect of grain refinement and reduce composites resistance to fracture. This result matches with studies of [63, 65]. On the other side, the effect of CF on ductility was noticeable where ductility is reduced as the weight fraction of CF increases due to the hard ceramic natures of CF. The 20 wt% uncoated CF composite has the lowest strain value, with 40.2% lower than the monolithic sample. Generally, CF could impede more deformations of composites under compression force.

It is also noticed that there is an improvement of compressive strength and ductility values for metal-coated CF/Al composites rather than uncoated ones. This improvement was small at low CF content and became significant at higher CF content. Improving the interfacial bonding between Al and CF and the homogenous distribution of reinforcement improved the load transfer from Al to CF and reduced the possibility of cracks. According to Orwan model, composites with agglomerated particles have higher interparticle spacing and lower strength than composites with uniform distribution ones [66]. Ductility of material depends on grain

Fig. 15 Compressive stress–strain diagram of pure Al and Al composites reinforced by CF with and without Cu coating
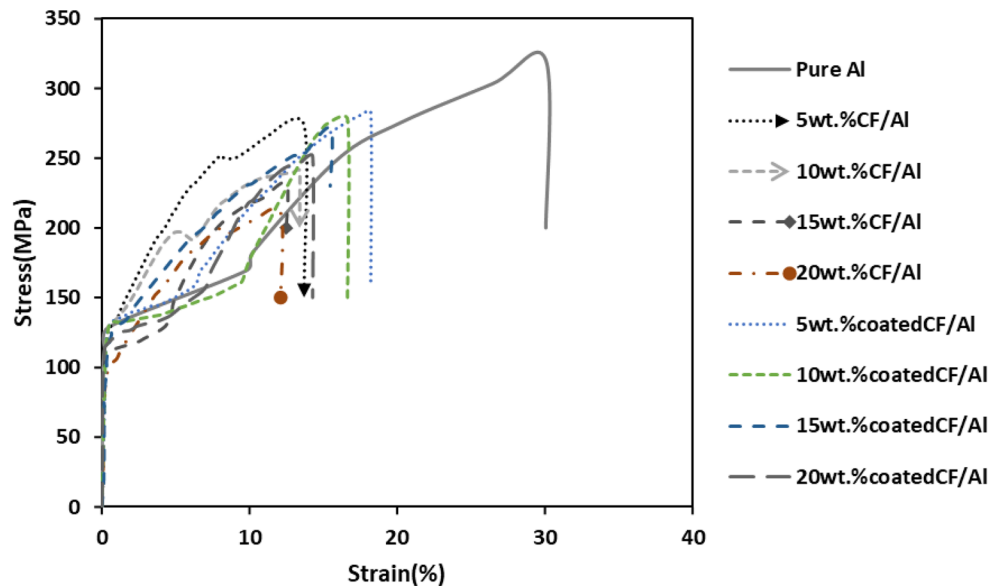

Table 5 The compression strength and elongation at fracture of CF/Al composites

Samples	Ultimate strength (MPa)	%Elongation (Ductility)
Pure Al	320.30	30.06
5 wt% CF/Al	273.78	13.70
10 wt% CF/Al	241.12	13.39
15 wt% CF/Al	232.22	12.49
20 wt% CF/Al	210.80	12.11
5 wt%Cu-coated CF/Al	282.94	18.21
10 wt%Cu-coated CF/Al	277.60	16.64
15 wt% Cu-coated/Al	271.76	15.46
20 wt% Cu-coated/Al	251.22	14.28

size, which ductility is reduced with increasing grain size [67]. So, the values of ductility of coated composites are higher compared to uncoated samples. Also, Agglomerated reinforcements significantly decrease the ductility of composites, as reported in the former studies [68, 69]. The uniform distribution of fiber in coated composites increases the ability to withstand deformation without fracture, resulting in large material elongations.

The microstructure of fracture surfaces of 20 wt% CF compression test samples were investigated to study further the coating layer's effect on fracture of composites. As shown in Fig. 16a, most CF is pulled out (marked as circles) in uncoated samples and extracted from the matrix, indicating the bonding between matrix and fiber at the interface was weak. In contrast, in coated composites, most of fiber is broken (marked as rectangular), as shown in Fig. 16b, suggesting the interfacial bonding was good. The strong interface between Cu-Al and Cu-fiber improved the load-bearing

capability of CF/Al composite at the interface through Cu nanoparticles. So, the mechanical properties of CF/Al composites depend on the interfacial bonding strength and the interaction between matrix and fiber.

3.9 Wear Rate Measurement

Figure 17 shows the effect of CF and the coating process on the specific wear rate of the prepared samples. It revealed that the wear rate decreases gradually by increasing CF percentage, and the coated samples have a lower wear rate than the uncoated ones. It is well known that hard ceramic particles result in improved wear behavior of AMC_S composites [70, 71]. In our study, the addition of CF into the Al matrix was an effective approach to enhance the wear properties of composites. The specific wear rate decreased as the weight fraction of CF increased, and this correlates to the literature [72, 73]. CF particles resist the micro-cutting of composites and restrain plastic deformation created by the cyclic load, so the wear rate of composites is decreased. The COF of composites in Fig. 18 follows the same trend, in which the COF of CF/Al composites is lower than the pure Al. CF usually acts as a self-lubricating film that restricts the direct contact between the sliding surface of composites and the counterpart. The incorporation of CF in the Al matrix enhances the wear resistance as CF has a lower density than Al, so it floats on the sample's surfaces, producing tribological layers that resist the wear and friction of samples. Jung et al. [74] stated similar results for CF/Al composites and observed that COF decreases as the mass of CF increases. Coated fiber could increase the load capacity of CF/Al composites due to improvement in wettability; thus, the COF and specific wear rate are reduced. The excellent adhesion and bonding between fiber and matrix are essential in systems
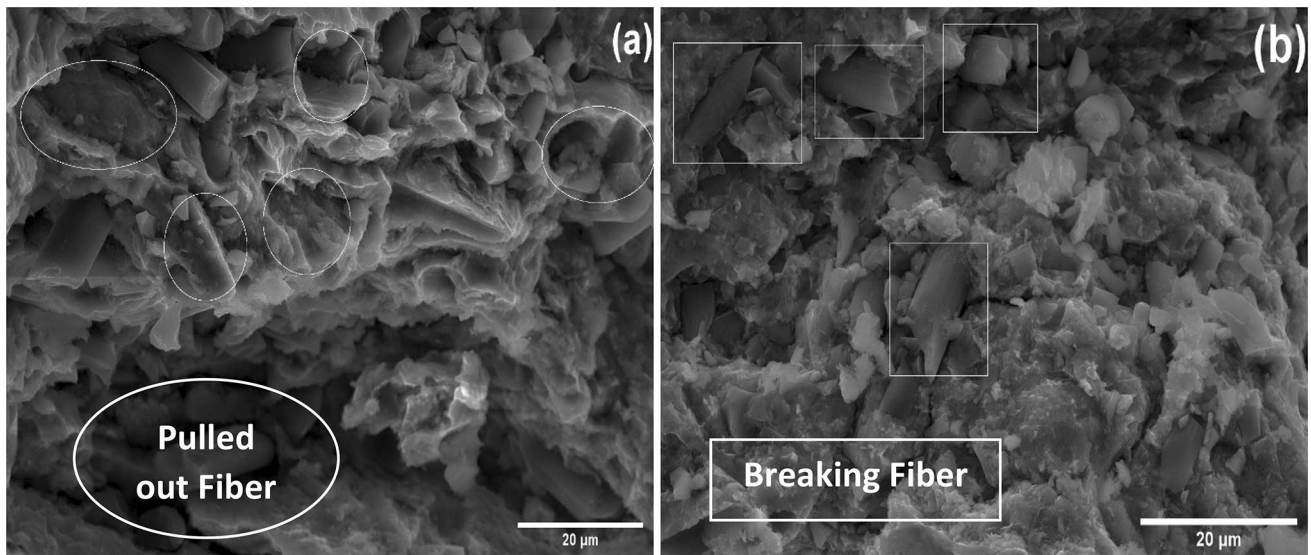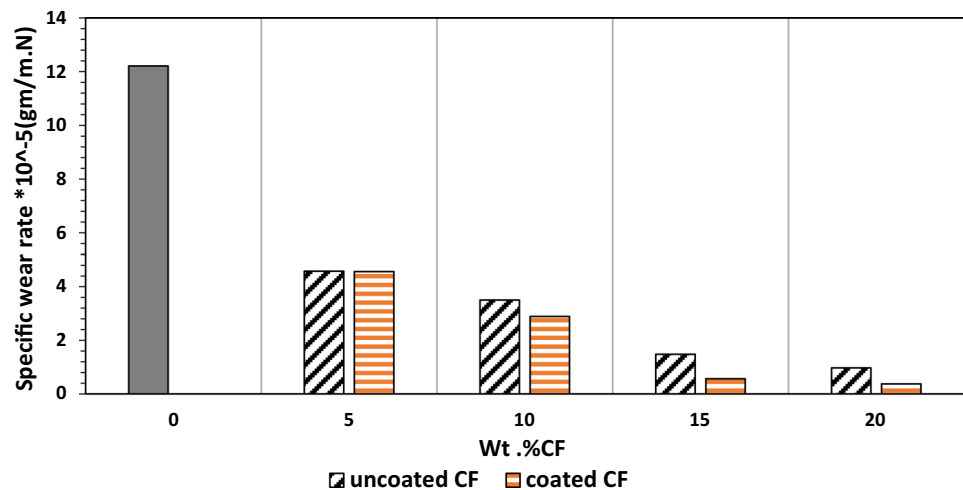
Fig. 16 Fractural microstructure of 20 wt% CF **a** uncoated composite, and **b** coated composite

Fig. 17 Specific wear rate of CF/Al composites

where wear mechanisms occur [75, 76]. As a general rule, the presence of coating layers on reinforcement displayed a better improvement in the tribological behavior of CF/Al composites.

The worn surfaces of unreinforced Al and composites reinforced with uncoated and coated CF at 10 wt% are presented in Fig. 19. The worn surface of the Al sample primarily contains grooves, wedges and microcracks. The delamination wear mechanism causes wedges and deep grooves, while the adhesive wear mechanism causes microcracks [71]. During the wear process, the friction force causes cyclic stresses on both sides of friction surfaces due to an increase in the temperature of the Al surface. This increase in temperature decreases the toughness and strength of Al, thereby severe plastic deformation

occurred, and some Al grains started to peel off, as shown in Fig. 19a. In contrast, the SEM micrograph of the worn surface of uncoated CF /Al composites reveals that longitudinal grooves are shallower and narrower compared to the pure sample. In addition, grain stripping and plastic deformation on the surface are weak. The previous observations indicated that the system turned from a high wear regime to an ultra-mild wear regime due to adding CF. It is also observed that fiber hasn't detached from the matrix and is distributed in a homogenous way in the sliding direction, which improves wear properties of composites, shown as in Fig. 19b. The previous observation is confirmed by the report [77]. Figure 19c shows that coated CF composites had the fewest grooves with some pits observed in the sample, thus coated CF/Al composites
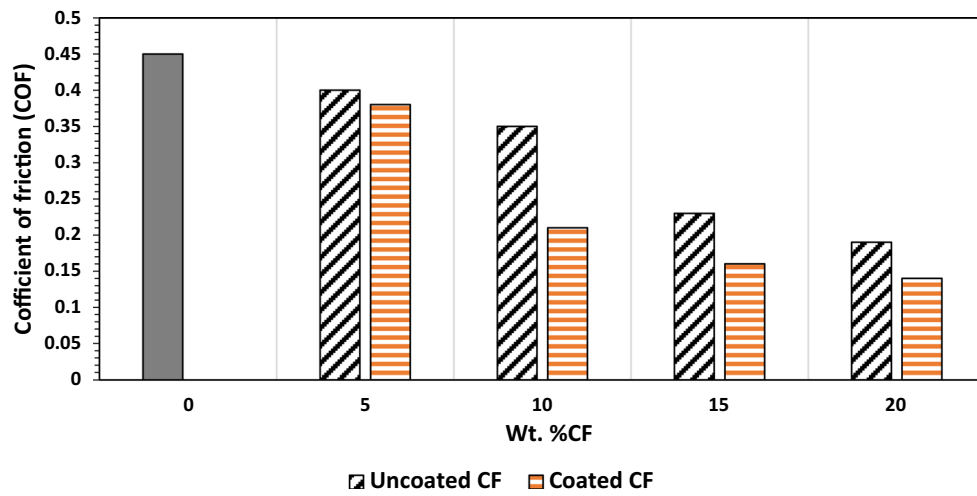
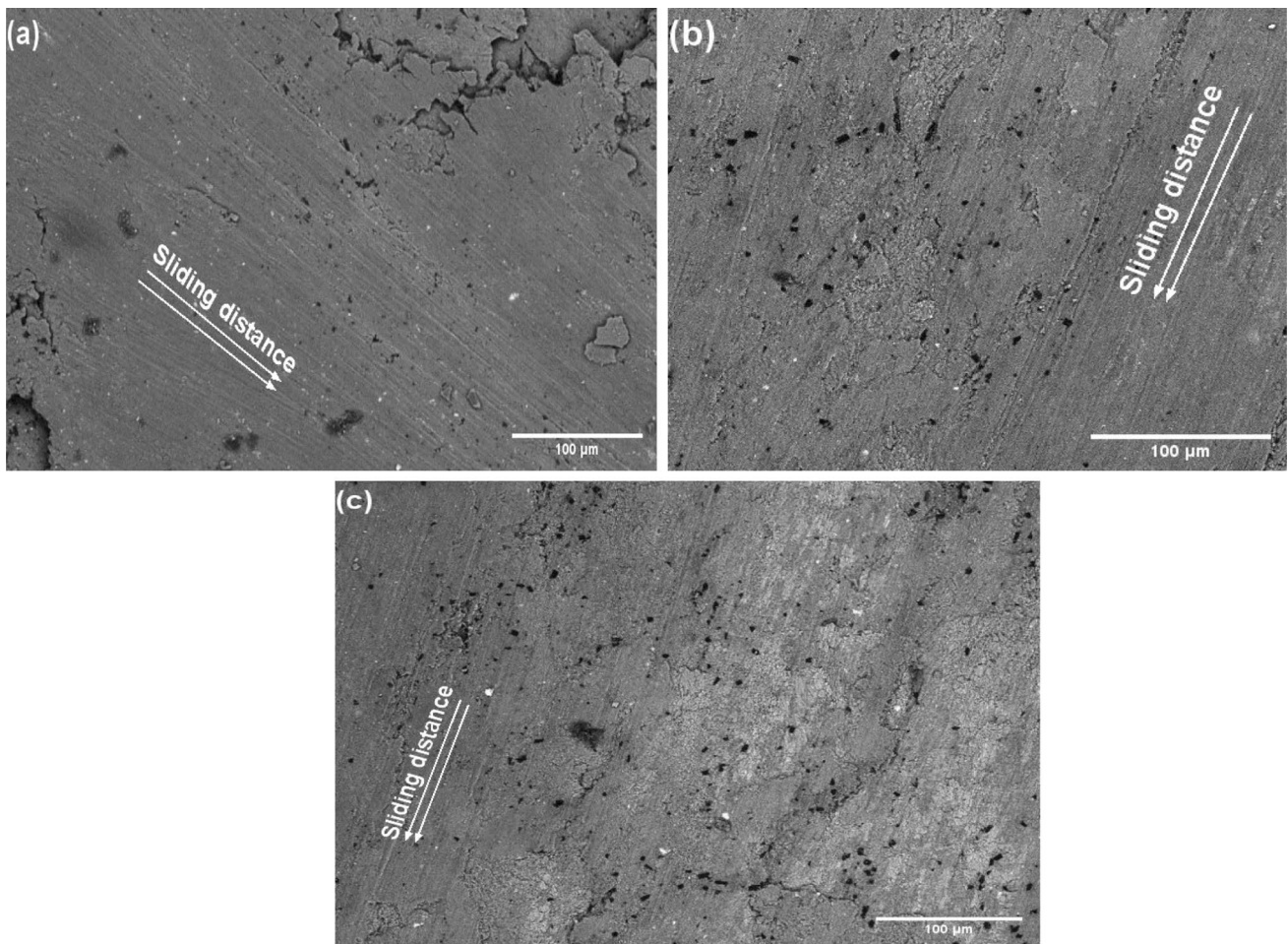Fig. 18 Coefficient of friction of CF/Al composites

Fig. 19 Worn surfaces of composites tested under 5 N with 1400 r/min **a** Pure Al powders, **b** 10 wt%CF/Al composites, and **c** 10 wt% Cu-coated CF/Al composites

had a lower wear rate and COF compared to uncoated and pure ones.

4 Conclusions

In this study, the authors aimed to solve the challenges of the fabrications of CF/Al composites through surface modification of CF surfaces by the nano Cu layer. In this investigation, 0, 5, 10, 15, and 20 wt% uncoated and Cu-coated CF /Al composites were successfully synthesized using the hot coining method. The composites are characterized by studying the microstructure, density, electrical, thermal and mechanical properties, considering the reinforcement content and electroless Cu coating process.

The results indicate that CF particles are uniformly distributed in Al matrix with some agglomerations in uncoated composites at a higher percentage of reinforcement. Moreover, nano Cu particles were effectively coated on CF surfaces and distributed between CF particles, contributing to the reduction of agglomerations and enhancing the interfaces between matrix and reinforcement. Also, XRD analysis of composites indicated that only Al and CF peaks were recorded, and also the absence of Al_4C_3 in all composites and Al_2Cu in coated composites. The relative density decreased with an increase in CF content due to micropores formations.

Increasing the amount of CF and using the nano Cu coated reinforcement reduced the CTE of composites. In addition, the electrical and thermal conductivities increased up to 10 wt% for uncoated CF composites and up to 15 wt% for coated composites. For uncoated composites, the hardness improved up to 10 wt% CF, while it continued to increase after 10 wt% CF when coated CF was used as reinforcement. Increasing CF content from 0 to 20 wt% caused a reduction in compressive strength for both uncoated and coated samples. The lowest value of compression strength was recorded at 20 wt% of uncoated CF/Al composite. Additionally, the incorporation of CF enhanced the wear resistance in the Al matrix, which specific wear rate and COF decreased as the CF content increased. In general, surface modification of CF with nano Cu layer was an effective way to improve the structure and thus, the electrical, thermal and mechanical properties of CF/Al composites are enhanced.

Declarations

Conflict of interest The authors declare that they have no conflict of interest.

References

1. C. Guo, X. He, S. Ren, X. Qu, J. Alloy. Compd. **664**, 777 (2016)
2. J. Cho, K.E. Goodson, Nat. Mater. **14**, 136 (2015)
3. A. Veillere, J.-M. Heintz, N. Chandra, J. Douin, M. Lahaye, G. Lalet, C. Vincent, J.-F. Silvain, Mater. Res. Bull. **47**, 375 (2012)
4. Y. Huang, Q. Ouyang, Q. Guo, X. Guo, G. Zhang, D. Zhang, Mater. Design **90**, 508 (2016)
5. W.W. Zhang, Y. Hu, Z. Wang, C. Yang, G.Q. Zhang, K.G. Prashanth, C. Suryanarayana, Mater. Sci. Eng. A **734**, 34 (2018)
6. A. Fathy, D. Ibrahim, O. Elkady, M. Hassan, J. Compos. Mater. **53**, 209 (2019)
7. R. Pei, G. Chen, Y. Wang, M. Zhao, G. Wu, J. Alloy. Compd. **756**, 8 (2018)
8. K. Shirvanimoghaddam, S.U. Hamim, M.K. Akbari, S.M. Fakhrhoseini, H. Khayyam, A.H. Pakseresht, E. Ghasali, M. Zabet, K.S. Munir, S. Jia, P. Davim, M. Naebe, Compos. Part A Appl. Sci. Manuf. **92**, 70 (2017)
9. H. Naji, S.M. Zebarjad, S.A. Sajjadi, Mater. Sci. Eng. A **486**, 413 (2008)
10. M. Eid, S. Kayetbay, O. Elkady, A. El-Assal, Ceram. Int. **47**, 21890 (2021)
11. M. Baghi, B. Niroumand, R. Emadi, J. Alloy. Compd. **710**, 29 (2017)
12. E. Hajjari, M. Divandari, A.R. Mirhabibi, Mater. Design **31**, 2381 (2010)
13. M.E. Abd EL-Maboud, S.M. Kayetbay, A.M. El-Assal, Am. J. Eng. Res. **10**, 134 (2021)
14. D.B. Miracle, Compos. Sci. Technol. **65**, 2526 (2005)
15. A. Luedtke, Adv. Eng. Mater. **6**, 142 (2004)
16. C. Zweben, Jom **50**, 47 (1998)
17. X. Peng, Y. Huang, X. Sun, X. Han, R. Fan, J. Mater. Sci. Mater. Electron. **30**, 7226 (2019)
18. S.-I. Oh, J.-Y. Lim, Y.-C. Kim, J. Yoon, G.-H. Kim, J. Lee, Y.-M. Sung, J.-H. Han, J. Alloy. Compd. **542**, 111 (2012)
19. X. Cao, Q. Shi, D. Liu, Z. Feng, Q. Liu, G. Chen, Compos. Part B Eng. **139**, 97 (2018)
20. Y. Huang, Q. Ouyang, D. Zhang, J. Zhu, R. Li, H. Yu, Acta Metall. Sin. Engl. **27**, 775 (2014)
21. Y. Tang, L. Liu, W. Li, B. Shen, W. Hu, Appl. Surf. Sci. **255**, 4393 (2009)
22. L.-F. Yi, T. Yamamoto, T. Onda, Z.-C. Chen, J. Compos. Mater. **54**, 2539 (2020)
23. S. Ghosh, Thin Solid Films **669**, 641 (2019)

24. J. Sudagar, J. Lian, W. Sha, J. Alloy. Compd. **571**, 183 (2013)
25. Y. Xue, W. Chen, Q. Zhao, Y. Fu, Surf. Coat. Tech. **358**, 409 (2019)
26. Y. Huang, X. Peng, Y. Yang, H. Wu, X. Sun, X. Han, Met. Mater. Int. **24**, 1172 (2018)
27. X. Peng, Y. Huang, X. Han, R. Fan, X. liu J. Alloy. Compd. **822**, 153584 (2020)
28. M. Eid, S. Kayetbay, O. Elkady, A. El-Assal, Int. J. Sci. Tech. Res. **10**, 122 (2021)
29. D. Jiang, X. Zhu, J. Yu, J. Wuhan Univ. Technol. **35**, 9 (2020)
30. Y. Huang, Y. Su, X. Guo, Q. Guo, Q. Ouyang, G. Zhang, D. Zhang, J. Alloy. Compd. **711**, 22 (2017)
31. M. Lee, Y. Choi, K. Sugio, K. Matsugi, G. Sasaki, Compos. Sci. Technol. **97**, 1 (2014)
32. T. Etter, P. Schulz, M. Weber, J. Metz, M. Wimmler, J.F. Löffler, P.J. Uggowitzer, Mater. Sci. Eng. A **448**, 1 (2007)
33. C. Zhang, Z. Cai, R. Wang, C. Peng, K. Qiu, N. Wang, Mater. Design **95**, 39 (2016)
34. N. Panwar, A. Chauhan, Mater. Today Proc. **5**, 5933 (2018)
35. S. Tahamtan, A. Halvaee, M. Emamy, M.S. Zabihi, Mater. Design **49**, 347 (2013)
36. J. Xiong, H. Zhang, Y. Peng, J. Li, F. Zhang, J. Therm. Spray Techn. **27**, 727 (2018)
37. O. El-Kady, A. Fathy, Mater. Design **54**, 348 (2014)
38. Z. Cai, C. Zhang, R. Wang, C. Peng, K. Qiu, Y. Feng, Mater. Design **87**, 996 (2015)
39. J. Rams, A. Urena, M.D. Escalera, M. Sanchez, Compos. Part A Appl. Sci. Manuf. **38**, 566 (2007)
40. M. Deshpande, R. Waikar, R. Gondil, S.V.S.N. Murty, T.S. Mahata, Processing of carbon fiber reinforced aluminium (7075) metal matrix composite, in *International Conference On Renewable Energy And Materials For Sustainability (ICREMS) 2016*, Noorul Islam Centre for Higher Education, Nagerkoil, 20-21 October 2016
41. A. Urena, J. Rams, M.D. Escalera, M. Sanchez, Compos. Sci. Technol. **65**, 2025 (2005)
42. A. Urena, J. Rams, M. Campo, M. Sanchez, Wear **266**, 1128 (2009)
43. ASTM B962-08, Standard Test Methods for Density of Compacted or Sintered Powder Metallurgy (PM) Products Using Archimedes' Principle (ASTM International, West Conshohocken, 2008)
44. A. Fathy, O. El-Kady, Mater. Design **46**, 355 (2013)
45. A. Fathy, F. Shehata, M. Abdelhameed, M. Elmahdy, Mater. Design **36**, 100 (2012)
46. W.S. Barakat, A. Wagih, O.A. Elkady, A. Abu-Oqail, A. Fathy, A. El-Nikhaily, Compos. Part B Eng. **175**, 107140 (2019)
47. Y. Li, R. Tian, Y. Xiao, W. Wang, X. Ding, L. Yin, J. Zhang, Mol. Cryst. Liq. Cryst. **651**, 273 (2017)
48. M.J. Yu, X.L. Cai, L. Zhou, C. Hu, Z. Li, F. Yi, Key Eng. Mater. **609-610**, 394 (2014)
49. M. Islam, M.R. Azhar, N. Fredj, T.D. Burleigh, O.R. Oloyede, A.A. Almajid, S.I. Shah, Surf. Coat. Tech. **261**, 141 (2015)
50. H. Xu, Z. Yang, M.-K. Li, Y.-L. Shi, Y. Huang, H.-L. Li, Surf. Coat. Tech. **191**, 161 (2005)
51. A. Fathy, O. Elkady, A. Abu-Oqail, Mater. Sci. Technol. **33**, 2138 (2017)
52. Y. Jia, F. Cao, S. Scudino, P. Ma, H. Li, L. Yu, J. Eckert, J. Sun, Mater. Design **57**, 585 (2014)
53. P.S. Turner, *The Problem of Thermal-Expansion Stresses in Reinforced Plastics* (National Advisory Committee for Aeronautics, United States,1942)
54. Y. Zhang, G. Wu, T. Nonferr. Metal. Soc. **20**, 2148 (2010)
55. I. Momohjimoh, N. Saheb, M.A. Hussein, T. Laoui, N. Al-Aqeeli, Ceram. Int. **46**, 16008 (2020)
56. O.A.M. Elkady, A. Abu-Oqail, E.M.M. Ewais, M. El-Sheikh, J. Alloy. Compd. **625**, 309 (2015)
57. O. El-Kady, H.M. Yehia, F. Nouh, Int. J. Refract. Met. Hard Mater. **79**, 108 (2019)
58. S.E. Shin, H.J. Choi, D. Bae, J. Compos. Mater. **47**, 2249 (2013)
59. T. Liu, X. He, L. Zhang, Q. Liu, X. Qu, J. Compos. Mater. **48**, 2207 (2014)
60. L.G. Hou, R.Z. Wu, X.D. Wang, J.H. Zhang, M.L. Zhang, A.P. Dong, B.D. Sun, J. Alloy. Compd. **695**, 2820 (2017)
61. G.E. Dieter, D.J. Bacon, *Mechanical Metallurgy* (McGraw-hill New York, 1988)
62. B.B. Singh, M. Balasubramanian, J. Mater. Process. Tech. **209**, 2104 (2009)
63. M.M.E.-S. Seleman, M.M.Z. Ahmed, S. Ataya, J. Mater. Sci. Technol. **34**, 1580 (2018)
64. F. Mokdad, D.L. Chen, Z.Y. Liu, D.R. Ni, B.L. Xiao, Z.Y. Ma, Mater. Sci. Eng. A **695**, 322 (2017)
65. M. Deshpande, R. Gondil, S.V.S.N. Murty, R.K. Kalal, T. Indian I. Metals **71**, 993 (2018)
66. Z. Hu, X. Li, H. Yan, X. Wu, H. Qun, J. Lin, J. Alloy. Compd. **685**, 58 (2016)
67. O.V. Rofman, A.V. Mikhaylovskaya, A.D. Kotov, A.G. Mochugovskiy, A.K. Mohamed, V.V. Cheverikin, M.P. Short, Mater. Sci. Eng. A **790**, 139697 (2020)
68. J. Segurado, C. Gonzalez, J. Llorca, Acta Mater. **51**, 2355 (2003)
69. S. Pourhosseini, H. Beygi, S.A. Sajjadi, Mater. Sci. Technol. **34**, 145 (2018)
70. A. Fathy, A. Abu-Oqail, A. Wagih, Ceram. Int. **44**, 22135 (2018)
71. N. Idusuyi, J.I. Olayinka, J. Mater. Res. Technol. **8**, 3338 (2019)
72. X.-L. Kong, Y. Liu, Y. Lu, B. Yang, Investigation of friction and wear behavior of carbon fiber felt reinforced aluminum-matrix composites. Tribology(China) **21**, 448 (2001)
73. L. Liu, W. Li, Y. Tang, B. Shen, W. Hu, Wear **266**, 733 (2009)
74. K.H. Jung, S. Nam, S.-S. Kang, B.-C. Ku, Y.H. Bang, J.Y. Hwang, Carbon Lett. **21**, 103 (2017)
75. S. Wilson, A.T. Alpas, Wear **225-229**, 440 (1999)
76. S.F. Moustafa, S.A. El-Badry, A.M. Sanad, B. Kieback, Wear **253**, 699 (2002)
77. Y.Q. Wang, J.I. Song, Wear **270**, 499 (2011)